Experimental Observation of Equilibrium and Dynamical Quantum Phase Transitions via Out-of-Time-Ordered Correlators

Xinfang Nie,[1,2,3,*] Bo-Bo Wei,[4,*] Xi Chen,[3] Ze Zhang,[1] Xiuzhu Zhao,[1] Chudan Qiu,[1] Yu Tian,[1] Yunlan Ji,[1] Tao Xin,[1,2,†] Dawei Lu,[1,2,‡] and Jun Li[1,2,§]

[1]*Shenzhen Institute for Quantum Science and Engineering and Department of Physics, Southern University of Science and Technology, Shenzhen 518055, China*

[2]*Guangdong Provincial Key Laboratory of Quantum Science and Engineering, Southern University of Science and Technology, Shenzhen 518055, China*

[3]*CAS Key Laboratory of Microscale Magnetic Resonance and Department of Modern Physics, University of Science and Technology of China, Hefei 230026, China*

[4]*School of Science and Engineering, The Chinese University of Hong Kong, Shenzhen, Shenzhen 518172, China*

(Received 26 December 2019; accepted 12 June 2020; published 22 June 2020)

The out-of-time-ordered correlators (OTOC), a fundamental concept for quantifying quantum information scrambling, has recently been suggested to be an order parameter to dynamically detect both equilibrium quantum phase transitions (EQPTs) and dynamical quantum phase transitions (DQPTs). Here we report the first experimental observation of EQPTs and DQPTs in a quantum spin chain via quench dynamics of OTOC on a nuclear magnetic resonance quantum simulator. We observe that the quench dynamics of the OTOC can unambiguously detect the DQPTs and the equilibrium critical point, while conventional order parameters such as the longitudinal magnetization can not. Moreover, we investigate the two-body correlations throughout the quench dynamics, and find that OTOC can extract the equilibrium critical point with higher accuracy and is more robust to decoherence than that of two-body correlation. Our experiment paves a way for experimentally investigating DQPTs through OTOCs and for studying the EQPTs through the nonequilibrium quantum quench dynamics with quantum simulators.

DOI: 10.1103/PhysRevLett.124.250601

Introduction.—Equilibrium quantum phase transitions (EQPTs) [1] are one of the most significant phenomena in many-body physics since it signals new states of quantum matter. It is accompanied by a nonanalytic change of some physical observable at a quantum critical point and is well understood from the paradigm of renormalization group theory [2]. Recently, dynamical quantum phase transitions (DQPTs) that emerge in the dynamics of an isolated quantum many-body systems have attracted extensive theoretical efforts [3–12] and experimental interests [13–19]. There are two different types of DQPTs. One type is witnessed by the nonanalyticity in the rate function of the Loschmidt echo at critical times [3], which resembles the nonanalyticity of free energy density as a function of temperature or other control parameters in the EQPTs. The other type is revealed by nonanalyticity of some local order parameters in quench dynamics measured at long time limit as a function of the control parameter of the quenched Hamiltonian [20–22]. Both types of DQPTs are intrinsically dynamical quantum phenomena without equilibrium counterparts [23].

EQPTs and DQPTs are both connected to the large quantum fluctuations [1,2] and therefore related to fast propagation of quantum information in many-body systems, which can be captured by a recently proposed out-of-time-ordered correlations (OTOC) [24–26]. OTOC is defined as

$$O(t) = \langle W(t)^\dagger V^\dagger W(t) V \rangle \tag{1}$$

for a given physical system described by a Hamiltonian H and an initial state $|\psi_0\rangle$. Here, W and V are two local Hermitian operators, where $W(t) = U^\dagger(t) W(0) U(t)$ is an operator in the Heisenberg picture with time evolution operator $U(t) = e^{-iHt}$, and $\langle\cdot\rangle$ denotes the expectation value over the initial state $|\psi_0\rangle$. OTOC has been proposed to describe dispersions of local quantum information in quantum many-body systems, termed "information scrambling" [26–37]. Moreover, it has triggered numerous applications in far-from-equilibrium quantum phenomena, ranging from nonequilibrium statistical mechanics [38], quantum thermalization [39–42] to black holes [43,44]. OTOC measurements have already been realized in a variety of systems, including nuclear magnetic resonance (NMR) [26] and trapped ions [45]. Recently, a theoretical study [46] suggested that quench dynamics of the OTOC can be used to detect EQPTs and DQPTs in many-body systems [47–49]. However, experimental progress on this OTOC-based detection scheme has been elusive.

Here, we report the first experimental observation of the EQPTs and DQPTs from the quench dynamics of OTOC. Specifically, we simulate short-range Ising models, including an integrable model and a nonintegrable model [46], on a four-qubit quantum simulator with the NMR technique. By measuring the quench dynamics of OTOC, we observe that it can clearly detect the DQPTs as well as the equilibrium critical points both in the integrable and nonintegrable Ising models. Autocorrelation function and two-body correlations are also measured for experimental comparison. It is found that autocorrelation function can not signal the DQPTs, and that while two-body correlations can also detect equilibrium critical points, it can not achieve the accuracy and robustness to decoherence as OTOC does. Therefore, our results experimentally establish OTOC as a useful probe of both EQPTs and DQPTs.

Quenches in Ising models.—We study the quench dynamics of ferromagnetic one-dimensional transverse-field Ising model with periodic boundary condition, as shown in Fig. 1(a). The corresponding Hamiltonian is written as

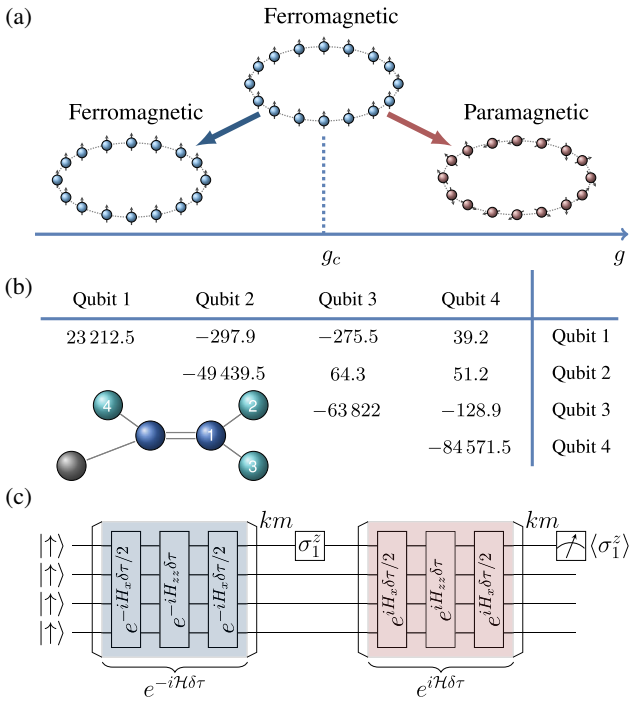

FIG. 1. (a) Illustration of the two kinds of sudden quantum quenches in a periodic one-dimensional ferromagnetic Ising chain from initial ferromagnetic phase to (i) ferromagnetic phase ($g < g_c$), and (ii) paramagnetic phase ($g > g_c$). (b) Molecular structure and the Hamiltonian parameters of ^{13}C-iodotrifluoroethylene (C_2F_3I). The precession frequencies ω_i and the scalar coupling strengths are given by the diagonal and off-diagonal elements in the table, respectively (units in Hz). (c) Quantum circuit diagram to detect the OTOC $F(t)$ of the one-dimensional Ising chains in experiments.

$$H = -\sum_{n=1}^{N}[J\sigma_n^z\sigma_{n+1}^z + \Delta\sigma_n^z\sigma_{n+2}^z + g\sigma_n^x], \tag{2}$$

where σ_n^α ($\alpha = x, y, z$) are Pauli operators on the nth site, J and Δ denote nearest-neighbor (NN) and the next-nearest-neighbor (NNN) couplings, and g is the uniform transverse field. For a ferromagnetic Ising model ($J > 0$), we assume $J = 1$ without loss of generality.

We investigate two kinds of Ising chains: the integrable version with only nearest interactions, i.e., $\Delta = 0$, which is termed as transverse-field Ising chain (TFIC), and the nonintegrable one with both NN and NNN interactions, namely axial next-nearest-neighbor Ising model (ANNNI). Both models serve as paradigms in EQPT [1,10,17,50–52]. The TFIC undergoes a quantum phase transition at the critical point $g_c = 1$: it stays in the ferromagnetic state for $g < 1$, and in the paramagnetic phase for $g > 1$. The quantum phase diagram is much more complex for the ANNNI [50–55]. Here, we consider the phase transition between ferromagnetic and paramagnetic phases in the case of $\Delta = 0.5$, where the critical point locates at $g_c \simeq 1.6$. The DQPTs in such Ising models have been theoretically and experimentally studied by Loschmidt echoes and two-body correlations [3,13,14,50].

DQPTs are usually investigated by quantum quenches. It starts from the ground state of an initial Hamiltonian H_0, and then evolves under another Hamiltonian H_f. For example, in the Ising model in Eq. (2), we choose $|\psi_0\rangle$ as the fully polarized state $|\uparrow\uparrow\uparrow\ldots\rangle$, which is one of the two degenerated ground states of initial Hamiltonian with $g = 0$. There are two kinds of quantum quenches in the transverse-field Ising model as shown in Fig. 1(a), depending on the case $g < g_c$ or $g > g_c$. DQPT only occurs in the second case when the system quenches across g_c.

The autocorrelation function $\chi(t) = \langle\sigma_n^z(t)\sigma_n^z\rangle$ [1], which can detect equilibrium dynamics, becomes indistinctive in the nonequilibrium case. It is proposed that the second moment of the autocorrelation function [46], i.e.,

$$F(t) = \langle\sigma_n^z(t)\sigma_n^z\sigma_n^z(t)\sigma_n^z\rangle, \tag{3}$$

can be used to distinguish the two kinds of quench dynamics. In fact, this function $F(t)$ corresponds to the OTOC $O(t)$ in Eq. (1) when the two local operators W and V are both chosen to be σ_n^z. In experiment, we set $W = V = \sigma_1^z$. Through observing the time dependence of $F(t)$, one can obtain the information about whether the time evolving Hamiltonian H is in the ferromagnetic or paramagnetic region. Moreover, the time-averaging OTOC $\bar{F} = (1/t)\int_{\tau=0}^{t} F(\tau)d\tau$ also serves as an order parameter for DQPT: $\bar{F}$ is nonzero for ferromagnetic phase and vanishes gradually upon approaching the critical point, while in contrast it stays zero in the whole paramagnetic phase. For comparison, the quench dynamics of the

two-body correlation $C(t) = \langle \sigma_1^z(t)\sigma_2^z(t)\rangle$ is also investigated in the experiment.

Experiment.—The experiments are carried out on a Bruker 600 MHz spectrometer. The physical system is the ensemble of ^{13}C-iodotrifluoroethylene (C_2F_3I) dissolved in d chloroform. This system has good performance in control, and was previously used for demonstrating the first OTOC measurement experiment [26]. The ^{13}C nuclear spin (Qubit 1) and the three ^{19}F nuclear spins (Qubits 2–4) constitute a four-qubit quantum simulator. Each nuclear spin corresponds to a spin site in the Ising model. The natural Hamiltonian of the sample is

$$H_{\mathrm{NMR}} = -\sum_{i=1}^{4}\frac{\omega_i}{2}\sigma_i^z + \sum_{i<j,=1}^{4}\frac{\pi J_{i,j}}{2}\sigma_i^z\sigma_j^z, \tag{4}$$

where $\omega_i/2\pi$ is the Larmor frequency of the ith spin, $J_{i,j}$ is the scalar coupling between the ith and jth spins. Molecular structure and the NMR Hamiltonian parameters of the sample are given in Fig. 1(b).

Because $|\psi_0\rangle$ is an eigenstate of σ_1^z, the OTOC in Eq. (3) can be rewritten as

$$F(t) = \langle \psi(t)|\sigma_1^z|\psi(t)\rangle, \tag{5}$$

with $|\psi(t)\rangle = e^{iHt}\sigma_1^z e^{-iHt}|\psi_0\rangle$. In other words, to measure the OTOC throughout the quench dynamics, we need to initialize the system to the fully polarized state $|\psi_0\rangle$, then apply a unitary transformation $U(t) = e^{iHt}\sigma_1^z e^{-iHt}$ and finally measure the expectation value $\langle\sigma_1^z\rangle$ of the final state. The whole experimental process is illustrated in Fig. 1(c). The experiment starts from a fully polarized state, and the method for implementing the desired time-reversal evolution is modified from the previous OTOC experiment [26]. The major task of the experiment is to simulate the unitary operation $U(t)$.

Given the target Hamiltonian H, we divide the quench dynamics into M discrete time steps, and record the instantaneous OTOCs at time $t = k\tau$ ($k = 0, 1\cdots M-1$). The unitary evolution $U(t)$ can be decomposed into a sequence of unitary transformations: a time evolution operator $e^{-iHk\tau}$, a single qubit rotation σ_1^z and a backward time evolution $e^{iHk\tau}$. The key point of the unitary evolution lies in the realization of the two operators $e^{-iH\tau}$ and $e^{iH\tau}$. Utilizing the Trotter-Suzuki decomposition formula, $e^{-iH\tau}$ can be simulated approximately by

$$e^{-iH\tau} \approx [e^{-iH_x\delta\tau/2}e^{-iH_{zz}\delta\tau}e^{-iH_x\delta\tau/2}]^m, \tag{6}$$

where the evolution time τ is divided into m segments with equal time length $\delta\tau = \tau/m$. Here, $H_x = -g\sum_{n=1}^{4}\sigma_x^n$, $H_{zz} = -\sum_{n=1}^{4}\sigma_z^n\sigma_z^{n+1}$ for the TFIC model, and $H_{zz} = -[\sum_{n=1}^{4}\sigma_z^n\sigma_z^{n+1} + \Delta\sum_{n=1}^{4}\sigma_z^n\sigma_z^{n+2}]$ for the ANNNI model. $e^{-iH_x\delta\tau/2}$ and $e^{-iH_{zz}\delta\tau}$ can be realized through optimized radio frequency pulses combined with the NMR refocusing technique. The reverse time evolution $e^{iH\tau}$ can also be done in a similar way. In experiment, to improve the control accuracy, we engineer the unitary evolution $U(t)$ with a shaped pulse optimized by the gradient ascent technique [56]. The width of the shaped pulse for each $U(t)$ is 40 ms with theoretical fidelity above 99.5%.

Integrable TFIC model.—We first study the quench dynamics in the TFIC. We consider two different quenches as shown in the upper panels of Fig. 1(a): (i) quenching from $g = 0$ to $g = 0.5$ and (ii) quenching from $g = 0$ to $g = 1.5$. The whole evolution is divided into $M = 12$ steps with fixed time increment $\tau = 0.5$, and the experimental results are shown in the upper panels of Fig. 2(a). Only the real parts of the OTOC $F(t)$ are measured in experiment. In both quenches, $F(t)$ starts from $F(t = 0) = 1$ at $t = 0$ and then decays due to the information spreading. Obviously, the long time behavior of the two cases are quite different. For $g = 0.5$ where the Hamiltonian is in the ferromagnetic region, $F(t)$ oscillates as a function of time but is always positive. In contrast, for $g = 1.5$, $F(t)$ oscillates around zero [57].

From the behavior of $F(t)$, we can readily differentiate the dynamical ferromagnetic phases and paramagnetic phases, i.e., there will be a DQPT in between. For comparison, we measure the time evolution of the autocorrelation $\chi(t) = \langle\sigma_1^z(t)\sigma_1^z\rangle$ and two-body correlation $C(t) = \langle\sigma_1^z(t)\sigma_2^z(t)\rangle$ during the quench dynamics, with the experimental results shown in the middle and lower panels of Fig. 2(a). The quantum circuit and the experimental procedure to measure $\chi(t)$ and $C(t)$ are put in the Supplemental Materials [58]. In theory, for quantum quench from the polarized state $|\uparrow\uparrow\uparrow\ldots\rangle$, $\chi(t) = \langle\sigma_1^z(t)\sigma_1^z\rangle = \langle\sigma_1^z(t)\rangle$ vanishes with time because the quantum system is heated by the quenching process. Indeed, we observe that $\chi(t)$ oscillates around zero in both quantum quenches [the middle panels of Fig. 2(a)], which indicates that the autocorrelation function and magnetization cannot be used to signify the two different dynamical quantum phases, and thus cannot detect DQPTs. The bottom panels of Fig. 2(a) show that the behavior of two-body correlation $C(t)$ is similar to that of OTOC $F(t)$ except that $C(t)$ oscillates around $1/2$ [13] for $g = 1.5$, which locates in the paramagnetic phase. Therefore, we have experimentally confirmed that the OTOC and two-body correlation can detect different dynamical quantum phases and the DQPTs, while the autocorrelation function cannot.

Furthermore, we study how the long-time average of OTOCs $\bar{F}$ changes with the transverse field g. We vary g from 0.1 to 1.9 with increment 0.1. The experimental results are shown in the top panel of Fig. 3(a). In the ferromagnetic phase, $\bar{F}$ is nonzero and eventually vanishes when approaching the equilibrium critical point $g = 1$. In the paramagnetic phase, $\bar{F}$ stays zero. This result confirms the validity of using the long-time averaged OTOC as an order parameter to

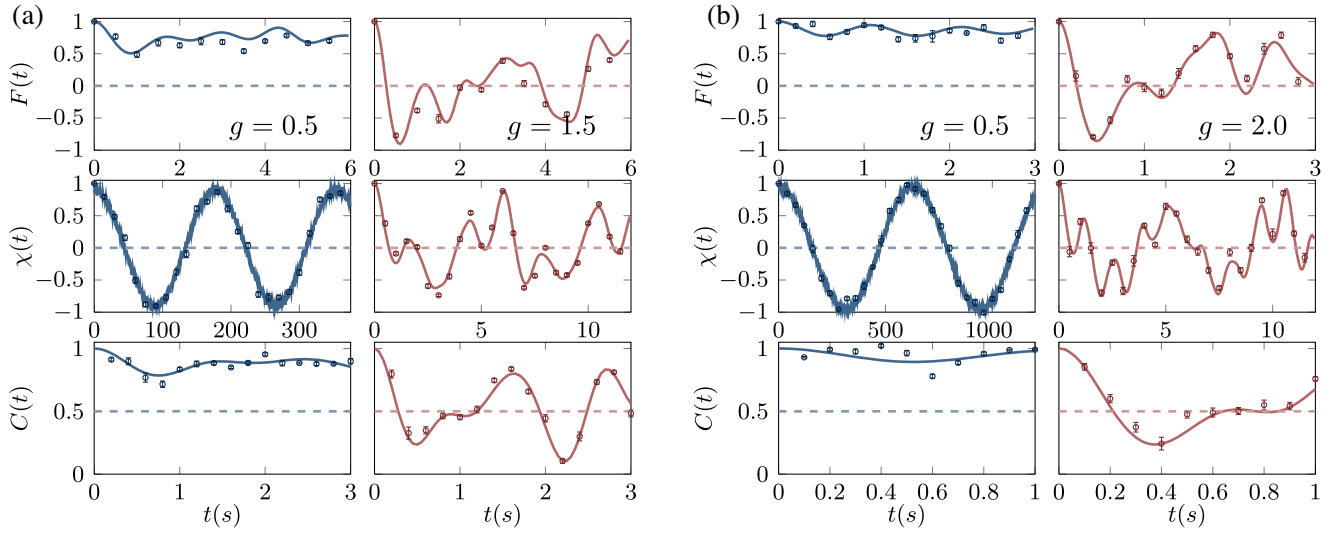

FIG. 2. Experimentally measured OTOC $F(t)$ (top panels), autocorrelation $\chi(t)$ (middle panels), and two-body correlation $C(t)$ (bottom panels) of the quantum quench dynamics as a function of time t in (a) TFIC model with $\Delta = 0$ and (b) ANNNI model with $\Delta = 0.5$. Both systems start from the fully polarized state $|\psi_0\rangle$ and then undergo evolutions governed by the Hamiltonian $H(g)$. The dots are the experimental data, the solid lines are the numerical simulation results, and the error bars are calculated from standard deviations of repeated experiments.

detect DQPTs as well as to locate the corresponding equilibrium quantum critical point. The fluctuation beyond the critical point in the simulation result (blue dashed line) is due to the small size of the system. We implement numerical simulations in larger systems ($N \geq 9$), and find that the fluctuation is much lower (red solid line). The experimental long-time average of two-body correlations $\bar{C}$ are shown in the bottom panel of Fig. 3(a), which indicates a phase transition near the equilibrium critical point but not as obvious as that of OTOC and stabilizes at $\bar{C} \to 1/2$ finally [13]. From both the experimental and numerical results of the two-body correlation and OTOC, it can be seen that OTOC gives a more accurate critical point than two-body correlation in the integrable TFIC model. Moreover, OTOC is also more robust against decoherence noise in detecting DQPTs by numerical simulations [58].

Nonintegrable ANNNI mode.—We now turn to the nonintegrable ANNNI model. Two different quantum quenches are investigated: from $g = 0$ to $g = 0.5$ and from $g = 0$ to $g = 2.0$. The dynamics is divided into $M = 15$ segments with duration of each segment set as $\tau = 0.2$. The experimental OTOCs $F(t)$ are shown in the top panels of Fig. 2(b), and the $\chi(t)$ and $C(t)$ are also measured for comparison, shown in the bottom panels of Fig. 2(b). From the results, it can be seen that, the autocorrelation function cannot distinguish different dynamical phases and the DQPTs, while the OTOC and two-body correlation work fine. The long-time averaged OTOC and two-body correlation as functions of the quenched parameter are experimentally observed in Fig. 3(b), where g is varied from 0.1 to 2.4. Similar behaviors with the TFIC model are observed for the ANNNI model: $\bar{F}$ takes a finite value at the ferromagnetic phase, gradually approaches zero when g approaches the critical point $g_c \simeq 1.6$, and finally stays zero throughout the paramagnetic region. This is an evidence that OTOC in quench dynamics can be served as an order parameter to locate the equilibrium quantum critical point in the nonintegrable cases, beating the autocorrelation function. The numerical simulation for $N = 9$ (red solid line) is also given. The result of two-body correlation is shown in the bottom panel of Fig. 3(b), it appears as a signature of phase transition near the critical point. The OTOC is a more precise probe of the critical point than that of two-body correlation in the nonintegrable

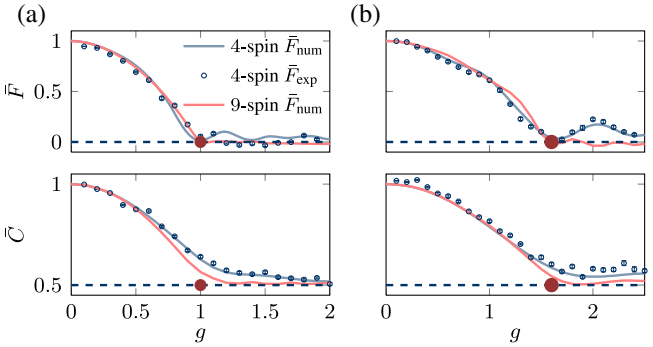

FIG. 3. Long-time averaged OTOC $\bar{F}$ (top panels) and two-body correlation $\bar{C}$ (bottom panels) as a function of the transverse field strength g in (a) TFIC model and (b) ANNNI model. The blue dots and the solid lines represent the experimental data and numerical simulation results, respectively. The red dots represent the phase transition critical points of the two models between the ferromagnetic phase and the paramagnetic phase, respectively. The red lines are the simulation results with $N = 9$ for comparison.

ANNNI Ising model, and is also more robust against decoherence than two-body correlation [58].

Conclusion.—In this Letter, we present the first experimental observation of EQPTs and DQPTs from quench dynamics of OTOC in both integrable and nonintegrable Ising models on an NMR quantum simulator. Therefore, our experiment unveils the important correlations between the OTOC and DQPTs. Moreover, our experiment demonstrates the feasibility of experimentally studying the EQPTs by performing a dynamical nonequilibrium measurement without carrying out the challenging initialization of the true many-body ground state. In addition to quantifying the information scrambling and diagnosing chaotic behavior of quantum many-body systems, our experiment establishes the OTOC as a faithful probe for DQPTs and EQPTs. The work here focuses on the short-range Ising model. To extend to long-range models, it turns out that much larger scale quantum simulators are necessary for detecting dynamical critical points with sufficient accuracy [58]. Therefore, for future work, we anticipate that the intriguing relations among OTOCs, EQPTs, and DQPTs for long-range interacting many-body systems of one and higher dimensions will be investigated via experimental platforms like trapped ions and Rydberg atoms.

This work was supported by the National Key Research and Development Program of China (Grant No. 2019YFA0308100), the National Natural Science Foundation of China (Grants No. 11975117, No. 11875159, No. 11905099, and No. U1801661), Science, Technology and Innovation Commission of Shenzhen Municipality (Grant No. JCYJ20180302174036418), Guangdong Basic and Applied Basic Research Foundation (Grant No. 2019A1515011383), and Guangdong Provincial Key Laboratory (Grant No. 2019B121203002). B. B. W. also acknowledges the President's Fund of the Chinese University of Hong Kong, Shenzhen.

[*]These authors contributed equally to this work.
[†]xint@sustech.edu.cn
[‡]ludw@sustech.edu.cn
[§]lij3@sustech.edu.cn

[1] S. Sachdev, *Quantum Phase Transitions* (Cambridge University Press, Cambridge, England, 2011).
[2] J. Cardy, *Scaling and Renormalization in Statistical Physics* (Cambridge University Press, Cambridge, England, 1996).
[3] M. Heyl, A. Polkovnikov, and S. Kehrein, Phys. Rev. Lett. **110**, 135704 (2013).
[4] M. Heyl, Phys. Rev. Lett. **113**, 205701 (2014).
[5] M. Heyl, Phys. Rev. Lett. **115**, 140602 (2015).
[6] F. Andraschko and J. Sirker, Phys. Rev. B **89**, 125120 (2014).
[7] J. C. Budich and M. Heyl, Phys. Rev. B **93**, 085416 (2016).
[8] Z. Huang and A. V. Balatsky, Phys. Rev. Lett. **117**, 086802 (2016).
[9] A. A. Zvyagin, Low Temp. Phys. **42**, 971 (2016).
[10] S. Sharma, U. Divakaran, A. Polkovnikov, and A. Dutta, Phys. Rev. B **93**, 144306 (2016).
[11] C. Karrasch and D. Schuricht, Phys. Rev. B **95**, 075143 (2017).
[12] L. Zhou, Q.-h. Wang, H. Wang, and J. Gong, Phys. Rev. A **98**, 022129 (2018).
[13] J. Zhang, G. Pagano, P. W. Hess, A. Kyprianidis, P. Becker, H. Kaplan, A. V. Gorshkov, Z.-X. Gong, and C. Monroe, Nature (London) **551**, 601 (2017).
[14] P. Jurcevic, H. Shen, P. Hauke, C. Maier, T. Brydges, C. Hempel, B. P. Lanyon, M. Heyl, R. Blatt, and C. F. Roos, Phys. Rev. Lett. **119**, 080501 (2017).
[15] X.-Y. Guo, C. Yang, Y. Zeng, Y. Peng, H.-K. Li, H. Deng, Y.-R. Jin, S. Chen, D. Zheng, and H. Fan, Phys. Rev. Applied **11**, 044080 (2019).
[16] K. Wang, X. Qiu, L. Xiao, X. Zhan, Z. Bian, W. Yi, and P. Xue, Phys. Rev. Lett. **122**, 020501 (2019).
[17] H. Bernien, S. Schwartz, A. Keesling, H. Levine, A. Omran, H. Pichler, S. Choi, A. S. Zibrov, M. Endres, M. Greiner, V. Vuletić, and M. D. Lukin, Nature (London) **551**, 579 (2017).
[18] N. Fläschner, D. Vogel, M. Tarnowski, B. Rem, D.-S. Lühmann, M. Heyl, J. Budich, L. Mathey, K. Sengstock, and C. Weitenberg, Nat. Phys. **14**, 265 (2018).
[19] T. Tian, Y. Ke, L. Zhang, S. Lin, Z. Shi, P. Huang, C. Lee, and J. Du, Phys. Rev. B **100**, 024310 (2019).
[20] B. Žunkovič, M. Heyl, M. Knap, and A. Silva, Phys. Rev. Lett. **120**, 130601 (2018).
[21] V. Zauner-Stauber and J. C. Halimeh, Phys. Rev. E **96**, 062118 (2017).
[22] J. C. Halimeh and V. Zauner-Stauber, Phys. Rev. B **96**, 134427 (2017).
[23] M. Heyl, Rep. Prog. Phys. **81**, 054001 (2018).
[24] S. H. Shenker and D. Stanford, J. High Energy Phys. 03 (2014) 067.
[25] S. H. Shenker and D. Stanford, J. High Energy Phys. 12 (2014) 046.
[26] J. Li, R. Fan, H. Wang, B. Ye, B. Zeng, H. Zhai, X. Peng, and J. Du, Phys. Rev. X **7**, 031011 (2017).
[27] Y. Chen, arXiv:1608.02765v2.
[28] S. Banerjee and E. Altman, Phys. Rev. B **95**, 134302 (2017).
[29] R.-Q. He and Z.-Y. Lu, Phys. Rev. B **95**, 054201 (2017).
[30] H. Shen, P. Zhang, R. Fan, and H. Zhai, Phys. Rev. B **96**, 054503 (2017).
[31] K. Slagle, Z. Bi, Y.-Z. You, and C. Xu, Phys. Rev. B **95**, 165136 (2017).
[32] R. Fan, P. Zhang, H. Shen, and H. Zhai, Sci. Bull. **62**, 707 (2017).
[33] Y. Huang, Y.-L. Zhang, and X. Chen, Ann. Phys. (Amsterdam) **529**, 1600318 (2017).
[34] E. Iyoda and T. Sagawa, Phys. Rev. A **97**, 042330 (2018).
[35] C.-J. Lin and O. I. Motrunich, Phys. Rev. B **97**, 144304 (2018).
[36] S. Pappalardi, A. Russomanno, B. Žunkovič, F. Iemini, A. Silva, and R. Fazio, Phys. Rev. B **98**, 134303 (2018).
[37] Y.-L. Zhang, Y. Huang, and X. Chen, Phys. Rev. B **99**, 014303 (2019).
[38] N. Yunger Halpern, Phys. Rev. A **95**, 012120 (2017).
[39] J. Eisert, M. Friesdorf, and C. Gogolin, Nat. Phys. **11**, 124 (2015).

[40] A. Bohrdt, C. B. Mendl, M. Endres, and M. Knap, New J. Phys. **19**, 063001 (2017).
[41] B. Swingle, Nat. Phys. **14**, 988 (2018).
[42] M. Campisi and J. Goold, Phys. Rev. E **95**, 062127 (2017).
[43] S. Grozdanov, K. Schalm, and V. Scopelliti, Phys. Rev. Lett. **120**, 231601 (2018).
[44] J. M. Magán, J. High Energy Phys. 09 (2018) 043.
[45] M. Gärttner, J. G. Bohnet, A. Safavi-Naini, M. L. Wall, J. J. Bollinger, and A. M. Rey, Nat. Phys. **13**, 781 (2017).
[46] M. Heyl, F. Pollmann, and B. Dóra, Phys. Rev. Lett. **121**, 016801 (2018).
[47] C. B. Dag, K. Sun, and L.-M. Duan, Phys. Rev. Lett. **123**, 140602 (2019).
[48] Z.-H. Sun, J.-Q. Cai, Q.-C. Tang, Y. Hu, and H. Fan, Ann. Phys. (Amsterdam) **532**, 1900270 (2020).
[49] B.-B. Wei, G. Sun, and M.-J. Hwang, Phys. Rev. B **100**, 195107 (2019).
[50] C. Karrasch and D. Schuricht, Phys. Rev. B **87**, 195104 (2013).
[51] W. Selke, Phys. Rep. **170**, 213 (1988).
[52] B. K. Chakrabarti, A. Dutta, and P. Sen, *Quantum Ising Phases and Transitions in Transverse Ising Models*, Vol. 41 (Springer Science & Business Media, Berlin, 2008).
[53] P. Ruján, Phys. Rev. B **24**, 6620 (1981).
[54] I. Peschel and V. J. Emery, Z. Phys. B **43**, 241 (1981).
[55] M. Beccaria, M. Campostrini, and A. Feo, Phys. Rev. B **73**, 052402 (2006).
[56] N. Khaneja, T. Reiss, C. Kehlet, T. Schulte-Herbrüggen, and S. J. Glaser, J. Magn. Reson. **172**, 296 (2005).
[57] This result is to some extent different in comparison to the theoretical prediction in Ref. [46], which states that $F(t)$ will reach zero. This discrepancy is mainly due to the small size of the simulated system; see the Supplemental Material [58].
[58] See the Supplemental Material at http://link.aps.org/supplemental/10.1103/PhysRevLett.124.250601 for experimental details and numerical simulations.